IMPACT OF BPL PENALTY FUNCTIONS AND PSF MODELS IN PET/CT RADIAL SPATIAL RESOLUTION RECOVERY

WANG JIE SI

SCHOOL OF HEALTH SCIENCES
UNIVERSITI SAINS MALAYSIA

2024

IMPACT OF BPL PENALTY FUNCTIONS AND PSF MODELS IN PET/CT RADIAL SPATIAL RESOLUTION RECOVERY

by

WANG JIE SI

Dissertation submitted in partial fulfilment of the requirements for the degree of Bachelor of Health Science (Honours) (Medical Radiation)

July 2024

ACKNOWLEDGEMENT

I would like to extend my heartfelt gratitude to Dr. Marianie Binti Musarudin, lecturer, in School of Health Sciences at Health Campus of Universiti Sains Malaysia for her exceptional guidance, unwavering support and invaluable insight throughout this journey. Her dedication and expertise in nuclear medicine field have been instrumental in shaping this research. Besides, I would also like to express my deeply thankful to Dr. Mohammad Aminudin Bin Said, the head physicist of Nuclear Medicine Department at National Cancer Institute, for providing me with all necessary facilities for the research. I could not have undertaken this research project without his vast expertise, continuous encouragement, invaluable opinion, and oversight. Moreover, I would like to express my gratitude to Dr. Mohammad Khairul Azhar Bin Abdul Razab, the lecturer at School of Health Science at Health Campus of University Sains Malaysia for his valuable feedback and encouragement, which have helped me navigate various challenges and refine my work. Special thanks go to Pn. Ummi Habibah Ibrahim, medical physicist at Nuclear Medicine Department at National Cancer Institute for her assistance in the data collection, practical insights, and continuous support during the fieldwork phase of this research. Additionally, I would like to thank my parents, family members and friends for their continuous mental, financial, moral support, and unwavering belief in my capabilities during the challenging phases of this research. Lastly, I acknowledge all those who have directly or indirectly contributed to this project.

TABLE OF CONTENTS

CERTIFICATE ..... **ii**

DECLARATION ..... **iv**

ACKNOWLEDGEMENT ..... **v**

TABLE OF CONTENTS ..... **vi**

LIST OF TABLES ..... **x**

LIST OF FIGURES ..... **xi**

LIST OF SYMBOLS ..... **xiv**

LIST OF ABBREVIATIONS ..... **xv**

LIST OF APPENDICES ..... **xvii**

ABSTRAK ..... **xviii**

ABSTRACT ..... **xx**

CHAPTER 1 INTRODUCTION **1**

1.1 Background of Study 1

1.2 Problem Statement 3

1.3 Study Objective 5

1.3.1 General Objectives 5

1.3.2 Specific Objective 5

1.4 Study Hypothesis 5

1.4.1 Null Hypothesis 5

1.4.2 Alternative Hypothesis 6

1.5 Significant of Study 6

1.6 Conceptual Framework 7

CHAPTER 2 LITERATURE REVIEW **8**

2.1 Operational Principle of PET/CT 8

2.2 Spatial Resolution in PET/CT Field of View (FOV) 8

2.3 Fundamental Limitations of PET/CT in Spatial Resolution 10
2.3.1 Natural Physical Limitation 11
2.3.1.1 Positron Range 11
2.3.1.2 Photon non-collinearity 12
2.3.2 Detector Related Effects 13
2.3.2.1 Width of scintillation crystals 13
2.3.2.2 Inter-crystal scattering and penetration 14
2.3.2.3 Decoding 15
2.3.2.4 Sampling Errors 16
2.4 Spatial Resolution Recovery by Reconstruction Algorithms 16
2.4.1 Ordered Subset Expectation Maximization (OSEM) Algorithm 17
2.4.2 Time of Flight (TOF) 18
2.4.3 Point Spread Function (PSF) Modelling 20
2.4.4 Bayesian Penalized Likelihood (BPL) 23
CHAPTER 3 METHODOLOGY 28
3.1 Study Design 28
3.2 Study Location 28
3.3 Materials 29
3.3.1 Discovery MI DR (2020) PET/CT Scanner 29
3.3.2 In-House Spatial Resolution Phantom 30
3.3.3 Capintec CRC-55tR Dose Calibrator 31
3.3.4 Radiotracer ^{18}F and Dye 32
3.3.5 3 mL Syringe with Needle and Beaker 33
3.3.6 Mirco-Hematocrit Capillary Tubes 33
3.3.7 Plastic Tray and Clay 34
3.3.8 Xeleris Functional Imaging Workstation Version 4.1 35
3.4 Methodology 36

3.4.1 Point Source Preparation and Phantom Setup 37
3.4.2 PET/CT Image Acquisition 39
3.4.3 PET/CT Image Reconstruction 41
3.4.4 Post Reconstruction Analysis 42
3.4.5 Data Analysis 44
3.5 Ethical Clearance 45
3.6 Study Flowchart 46
CHAPTER 4 RESULT AND DISCUSSION 47
4.1 Effect of Radial Distance on Spatial Resolution in PET/CT FOV 47
4.1.1 Tangential FWHM 47
4.1.2 Radial FWHM 49
4.1.3 Data Analysis 50
4.1.4 Discussion 51
4.2 Ability of PSF Modelling and Beta Penalization Function in OSEM Algorithm to Retain Spatial Resolution Within PET/CT FOV 53
4.2.1 Tangential FWHM 53
4.2.2 Result of Radial FWHM 56
4.2.3 Data Analysis 59
4.2.4 Discussion 60
4.3 Optimization of Beta Values for BPL in OSEM Algorithm across Different Radial Distances of PET/CT FOV 61
4.3.1 Tangential FWHM 62
4.3.2 Radial FWHM 64
4.3.3 Data Analysis 66
4.3.4 Discussion 68
4.4 Limitations of Study 71
CHAPTER 5 CONCLUSION AND FUTURE RECOMMENDATIONS 74
5.1 Conclusion 74

5.2 Recommendations for Future Research 75

REFERENCES 77

APPENDICES 84

APPENDIX A 84

APPENDIX B 85

LIST OF TABLES

Page

Table 2.1 Characteristic of Commonly Used Positron Emitting Isotopes (Kevrešan, n.d.). 12

Table 2.2: Different terminology for different image reconstruction methods coined by different vendors. 17

Table 2.3: Different beta values employed for different studies. 26

Table 3.1: Types of reconstruction techniques employ in the study. 36

Table 4.1: Tangential FWHM (mm) computed at radial distances ranges from 5 to 20 cm from the center of the PET/CT FOV. Measurements were performed at four locations from the center (A to D). 47

Table 4.2: Radial FWHM (mm) computed at radial distances ranges from 5 to 20 cm from the center of the PET/CT FOV. Measurements were performed at four locations from the center. 49

LIST OF FIGURES

Page

Figure 1.1: Conceptual framework 7

Figure 2.1: Different type of medium in affecting positron range (Herraiz et al., 2020). 12

Figure 2.2: Basic principle of PET with occurrence of photon non-collinearity (Jiang et al., 2019). 13

Figure 2.3: (a) Inter-crystal Scattering; (b) Inter-crystal Penetration (Iriarte et al., 2015) 15

Figure 2.4: LORs in PET camera (Moses, 2011) 16

Figure 2.5: Concept of TOF PET and Non-TOF PET (Jiang et al., 2019). 20

Figure 2.6: ^{68}Ga-prostate-specific membrane antigen (PSMA) PET images that shows the uptake of PSMA in prostate and four metastases. PET data is reconstructed with (a) OSEM, (b) OSEM+PSF and (c) OSEM+TOF+PSF (van der Vos et al., 2017). 21

Figure 2.7: Top row shows the 100 million counts acquisition of NEMA image quality while bottom row shows the ^{18}F–FDG PET images of ovarian cancer patient with peritoneal carcinomatosis. Both rows of PET data are reconstructed with (a) OSEM, (b) OSEM+ TOF+PSF and (c) OSEM+TOF+PSF+BPL (β400) (van der Vos et al., 2017). 25

Figure 3.1: Discovery MI DR (Digital-Ready PET/CT Scanner) 29

Figure 3.2: Design of in-house spatial resolution phantom 30

Figure 3.3: (a) In-house spatial resolution; (b) In-house spatial resolution was placed on the phantom holder 31

Figure 3.4: Dose Calibrator 32

Figure 3.5: (a) Radiotracer ^{18}F is sealed in a lead container; (b) Dye was added into 18F radiotracer 32

Figure 3.6: Syringe and beaker 33

Figure 3.7: Mirco-Hematocrit Capillary Tubes 34

Figure 3.8: (a) Plastic tray that consist of a few equal sized drops; (b) Clay was used to sealed end of capillary tube. 34

Figure 3.9: Xeleris Functional Imaging Workstation Version 4.1.....36

Figure 3.10: (a) Activity of radiotracer ^{18}F measured; (b) Equal sized drops were prepared using a syringe with needle. 38

Figure 3.11: Source was drawn into capillary tube to form a point source and end of capillary tube was sealed with clay.....39

Figure 3.12: (a) Set up of the phantom and phantom was aligned with external and internal laser; (b) Capillary tube was positioned at 5 cm from the center of phantom in Location A. 39

Figure 3.13: (a) Default setting for scout scan; (b) Default setting for CT scan.....40

Figure 3.14: (a) Each point source underwent a one-minute scan; (b) Point source was scanned with 1 minute per one bed position. 40

Figure 3.15: (a) Interface of type of PET reconstruction techniques; (b) Default settings set for filter cut off, iteration and subsets. 42

Figure 3.16: Reconstruction parameters were selected for (a) OSEM+TOF+PSF and (b) OSEM+TOF+PSF+BPL. 42

Figure 3.17: (a) Central slice of PET/CT image for point source was selected (b) followed by ROI is created in horizontal direction to obtain tangential FWHM.....43

Figure 3.18: (a) ROI created in vertical direction to obtain radial FWHM; (b) Peak of the line profile. 43

Figure 3.19: Study Flowchart.....46

Figure 4.1: Graph of Radial Distances (cm) of Different Locations vs Tangential FWHM 48

Figure 4.2: Graph of Radial Distances (cm) of Different Locations vs Radial FWHM 50

Figure 4.3: Tangential FWHM measured using different reconstruction techniques (a) Location A (b) Location B (c) Location C (d) Location D.....55

Figure 4.4: Radial FWHM measured using different reconstruction techniques (a) Location A (b) Location B (c) Location C (d) Location D. 58

Figure 4.5: Tangential FWHM measured using different beta values (a) Location A (b) Location B (c) Location C (d) Location D. 63

Figure 4.6: Radial FWHM measured using different beta values (a) Location A (b) Location B (c) Location C (d) Location D. 66

Figure 4.7: Delineation of line structures on PET/CT images to measure FWHM. ..72

Figure 4.8: Fit line profiles into a Gaussian function using MATLAB R2023b. 72

LIST OF SYMBOLS

^{12}C	Carbon-12
^{18}F	Fluorine-18
^{18}F-FDG	Fludeoxyglucose Fluorine-18
^{68}Ga	Galium-68
^{68}Ga-PSMA	Galium-68 Prostate-Specific Membrane Antigen
^{13}N	Nitrogen-13
^{15}O	Oxygen-15
^{82}Rb	Rubidium-82

LIST OF ABBREVIATIONS

BPL	Bayesian Penalized-Likelihood
BSREM	Block Sequential Regularized Expectation Maximization
FOV	Field of View
FBP	Filter Back Projection
FHWM	Full Width Half Maximum
FORE	Fourier rebinning plus FBP
ICS	Inter-crystal scatter
ICP	Inter-crystal penetration
IEC	International Electrotechnical Commission
IKN	Institut Kanser Negara
LBS	Lutetium-based Scintillator
LOR	Line of Response
LSF	Line Spread Function
LSO	Lutetium Oxyorthosilicate
LYSO	Lutetium Yttrium Oxyorthosilicate
MREC	Medical Research and Ethics Committee (MREC)
MOH	Ministry of Health
NCI	National Cancer Institute
NEMA	National Electrical Manufacturers Association
OSEM	Ordered Subset Expectation Maximization
PET	Positron Emission Tomography
PET/CT	Positron Emission Tomography / Computed Tomography

PSF	Point Spread Function
PVE	Partial Volume Effect
RC	Recovery Coefficient
ROI	Region of Interest
RPC	Radiopharmaceutical
SBR	Sphere-to-Background Ratios
SNR	Signal to Noise Ratio
SUV	Standardized Uptake Value
VPHD	Vue Point HD
VPFX	Vue Point FX
TOF	Time of Flight

LIST OF APPENDICES

Appendix A	Ethical Approval Letter from MREC under MOH
Appendix B	Technical specification of PET/CT Scanner (a) PET Specifications and (b) CT Specifications (*Discovery MI DR*, 2020)

PENGARUH FUNGSI PENALTI BPL DAN MODEL PSF DALAM PEMULIHAN PELERAIAN RUANG RADIAL PET/CT

ABSTRAK

Pengenalan: Kaedah konvensional tiga sumber titik berpandukan garisan panduan NEMA NU 2-2018 diperkenalkan dengan menempatkan tiga sumber titik pada 1 cm, 10 cm, dan 20 cm dalam PET/CT FOV untuk menilai kesan jarak radial terhadap peleraian ruang. Pembentukan semula algoritma termaju seperti TOF, BPL, dan model PSF bersama OSEM menunjukkan peningkatan peleraian ruang kerana gabungan OSEM dan TOF meningkatkan penempatan peristiwa manakala model PSF menangani kesan paralaks. Walau bagaimanapun, OSEM sering mengalami kesukaran untuk mencapai penumpuan penuh, menyebabkan penggunaan BPL dengan fungsi penalti (nilai β) untuk pembinaan semula beriterasi yang diatur. Oleh kerana OSEM+TOF+PSF+BPL (β450) adalah protokol pengimejan semasa yang diamalkan oleh Institut Kanser Negara (IKN), kajian ini bertujuan untuk meneroka keberkesanan fungsi penaliti BPL alternatif dan pemodelan PSF dalam algoritma OSEM dalam meningkatkan peleraian ruang dalam FOV PET/CT dan menentukan nilai β yang optimum untuk pengimejan klinikal rutin. **Kaedah:** Kajian peleraian ruang menggunakan sumber titik F-18 tunggal dengan aktiviti >5mCi/cc telah diimplementasikan dengan menggunakan tiub kapilari untuk menarik titisan supaya menghasilkan sumber titik dengan isipadu 1 mm^3. Tiub kapilari tersebut diperuntukkan pada jarak radial yang berbeza dengan selang 5 cm dari pusat ke arah hujung PET/CT FOV. Pengimejan fantom dijalankan dengan pandangan scout, diikuti dengan pengimejan aksial CT dan PET selama 1 minit untuk setiap kedudukan katil. Data PET seterusnya direkonstruksi dengan OSEM+TOF, OSEM+TOF+PSF, dan

OSEM+TOF+PSF+BPL (β 200, 400, 450, 600, 800, 1000, dan 1200). FWHM tangensial dan radial sumber titik selanjutnya dikira dengan Xeleris Functional Imaging Workstation Versi 4.1. Pengaruh jarak radial terhadap peleraian ruang di bawah protokol IKN (OSEM+TOF+PSF+BPL dengan β450) dan nilai β BPL yang berbeza (β 200-1200) dinilai berdasarkan nilai kecerunan fungsi. Selain itu, kesan pelbagai algoritma rekonstruksi terhadap peleraian ruang dalam PET/CT FOV dinilai dengan pengiraan sisihan piawai dan membuat error bar untuk menunjukkan sebaran data sekitar min serta untuk menentukan perbezaan ketara antara FWHM yang diukur dengan pelbagai jenis algoritma rekonstruksi. **Keputusan:** Hanya FWHM tangensial di lokasi D mengikuti ramalan teori iaitu peningkatan FWHM dengan peningkatan jarak radial dalam FOV PET/CT dari 1.10 mm hingga 1.76 mm (R^2 = 0.8602). Selain itu, algoritma OSEM+TOF+PSF+BPL memberikan peleraian ruang terbaik berbanding OSEM+TOF dan OSEM+TOF+PSF, di mana BPL dengan β200 menghasilkan pengukuran FWHM yang lebih rendah. Oleh itu, kajian ini mencadangkan nilai β yang lebih rendah, dengan β200 sebagai pilihan optimum untuk mengekalkan peleraian ruang. **Kesimpulan:** Algoritma pemulihan OSEM+TOF+PSF+BPL (β200) dicadangkan sebagai pilihan optimum untuk IKN dalam pengimejan kinikal kerana algoritma ini menunjukkan kestabilan tertinggi dalam pemulihan peleraian ruang radial dengan peningkatan jarak radial.

IMPACT OF BPL PENALTY FUNCTION AND PSF MODELS IN PET/CT RADIAL SPATIAL RESOLUTION RECOVERY

ABSTRACT

Introduction: A conventional three-point source method adhering to NEMA NU 2-2018 has been introduced where three-point sources are placed at 1 cm, 10 cm, and 20 cm within the PET/CT FOV to evaluate impact of radial distance on spatial resolution. Advanced reconstruction algorithms like TOF, BPL, and PSF models, along with OSEM have shown spatial resolution enhancements based on the FWHM measured. Combining OSEM with TOF improves event localization, and PSF modelling mitigates parallax effects. However, OSEM often struggles with full convergence, necessitating BPL with smooth penalty functions (β values) for regularized iterative reconstruction. Since National Cancer Institute (NCI) currently practice OSEM+TOF+PSF+BPL (β 450) as the in-house protocol, this study explores alternative BPL and PSF functions in OSEM to enhance spatial resolution and determine optimal β values for NCI's routine clinical use. **Methods:** In-house spatial resolution phantom acquisition was conducted using single F-18 point source method with activity > 5mCi/cc. A capillary tube was used to draw the selected drop, creating the point source with volume 1 mm^3. Tubes filled were placed at 5 cm intervals from the center towards the PET/CT FOV's periphery. Scans were done with default settings of scout view, followed by CT axial slice scan and subsequently PET scan with 1 minute per bed position. PET data was then reconstructed with OSEM+TOF, OSEM+TOF+PSF, and OSEM+TOF+PSF+BPL (β 200,400,450, 600,800,1000 and 1200). Tangential and radial FWHM of the point source at different radial distances and locations were calculated by using Xeleris Functional Imaging Workstation

Version 4.1. Radial distance effects on spatial resolution under the NCI protocol (OSEM+TOF+PSF+BPL with β450) and varying BPL β values (β 200-1200) were evaluated using fitted function slopes. Additionally, different reconstruction algorithms' impact on spatial resolution within PET/CT FOV was assessed using standard deviation calculations and plotting error bars to show spreading of the data around the mean as well as to determine the significant difference between the FWHM measured using different types of reconstruction. **Result:** The tangential FWHM at Location D was the only measurement that aligned with the theoretical prediction, increasing linearly with the increment of the radial distance from 1.10 mm to 1.76 mm (R^2 = 0.8602). Additionally, OSEM+TOF+PSF+BPL provided greatest spatial resolution compared to OSEM+TOF and OSEM+TOF+PSF, where BPL with β200 reduced FWHM measurements closed to actual size of point source. **Conclusion:** OSEM+TOF+PSF+BPL (β200) reconstruction algorithms is suggested to be the optimum reconstruction algorithm that can be practiced by NCI in clinical setting due to best radial spatial resolution recovery even with increased of radial distances.

CHAPTER 1

INTRODUCTION

1.1 Background of Study

In Nuclear Medicine, Positron Emission Tomography (PET) is the second major method for tomographic imaging (Gabriel Reynes-Llompart, 2019). PET is a medical diagnostic technique that measures metabolic activity, pathology, and physiological function by looking at metabolism, neurotransmitters radiolabelled drugs and blood flow of the human body (Cherry et al., 2012). Since PET alone provides functional information with little information regarding the exact locations of suspicious lesions, PET images are later co-registered with CT to obtain good anatomical information and good spatial resolution.

Good spatial resolution is pivotal in image analysis accuracy as it can enhance clinical decision-making by providing more accurate diagnosis and treatment planning. Spatial resolution is defined as the ability of the PET/CT imaging system to distinguish between two separate objects that are close together in space (Moses, 2011). Small lesions within the body can also be identified with high spatial resolution which is crucial for the early detection of disease. Moreover, partial volume effect (PVE) might happen in PET scanners which results in low spatial resolution. Due to spillover from activity, this PVE will make tiny lesions appear larger and cause radiopharmaceutical (RPC) uptake to appear lower than actual values. (Braune et al., 2022; van der Vos et al., 2017).

Voxel size is also an important factor in determining spatial resolution in PET imaging. Large voxel size will produce more homogeneous images but result in low spatial resolution. In clinical practice, large image voxel sizes are typically desired to

obtain more counts per voxel and minimise image noise, but this eventually results in low spatial resolution of images. Hence, recent advances in PET technology like TOF and PSF modelling that utilize the smaller voxels have further improved image spatial resolution and subsequently improved small lesions detection (Shekari et al., 2017).

Radial distance in a PET/CT scanner is defined as the distance from the center of the PET scanner to the point of interaction on the PET scanner detector ring or PET/CT FOV periphery (O. Mawlawi et al., 2004). Spatial resolution in PET scanners is normally affected by radial offset. Theoretically, the spatial resolution degrades from the center towards the periphery of the FOV. Research by Smith et al. (2023) found that using F-18 point sources at radial offsets of 1 cm, 10 cm, and 20 cm as well as reconstructing images with OSEM algorithms per NEMA NU 2-2018 standards resulted in tangential FWHM values of 3.76 mm, 3.85 mm, and 4.19 mm, respectively, demonstrating that spatial resolution decreases with increasing radial distance.

PET scanners have experienced evolution to enhance fundamental changes in their design to new reconstruction and data processing methods. To improve spatial resolution, there is a rise in various iterative reconstruction algorithms such as Ordered Subset Expectation Maximization (OSEM) and Block-Sequential Regularized Expectation Maximization (BSREM). OSEM is an iterative algorithm that reconstructs PET images in which the data is divided into subsets and updates the image estimate after each subset is processed and it is mostly used nowadays (Kamiya et al., 2016). It can produce high quality images with relatively low computational cost (Lantos et al., 2018). Nevertheless, as the number of iterations increases, noise levels rise, limiting the ability to achieve complete quantitative convergence.

To improve the performance of OSEM by preserving the image quality and improving the PET quantitative accuracy, Bayesian Penalized-Likelihood (BPL) known as Q.Clear is a reconstruction that improves signal and reduces noise without compromising image quality, aiding in small lesion detection and providing consistent SUV measurements. BPL is BSREM that is based on OSEM but includes a penalty function (β value) which is possible for user input to improve the image quality (Kamiya et al., 2016; Lantos et al., 2018).

Besides BPL with different penalty functions, Point Spread Function (PSF) modelling is introduced which includes the modelling of resolution degrading phenomena. It is used to model the blurring effect of the scanner, thus resulting in the improvement of spatial resolution within the FOV and does not affect the quantitative values (Huang et al., 2021; Murata et al., 2016). PSF modelling can also improve the detection rates for small lesions and the signal-to-noise ratio (SNR) of PET imaging (Hotta et al., 2018). Moreover, the implementation of TOF in the OSEM algorithm allows localization of the point of annihilation on the line of response (LOR) which can help to improve lesion detectability and structural definition.

Since NCI is currently employing OSEM+TOF+PSF+BPL(β450) as standard routine clinical imaging protocol, this study aims to investigate whether alternative TOF, PSF modelling and BPL penalty functions in OSEM algorithms enhance the spatial resolution across PET/CT FOV while determining optimal β values for routine clinical use in NCI.

1.2 Problem Statement

Despite advancements in PET/CT imaging technology, spatial resolution is still degraded from center towards the periphery of PET/CT FOV which potentially

compromises diagnostic accuracy. Advanced reconstruction algorithms such as TOF, PSF modelling and BPL algorithms with penalty functions (β values) shown to improve the spatial resolution and image quality, but their efficacy in retaining spatial resolution, particularly at the periphery of PET/CT FOV remains underexplored. There is also a lack of comprehensive comparison between PSF modelling and BPL particularly with varying β values in OSEM algorithms to retain the spatial resolution within the PET/T FOV.

Furthermore, most of the studies employ the BPL with different β values to evaluate noise suppression, small lesion detectability and standardized uptake value (SUV) recovery. However, there is a deficiency in research assessing the FWHM of point sources using BPL with different penalty functions. Additionally, there is insufficient evidence on the impact of increasing β values of the BPL algorithm across different radial distance within the PET/CT FOV. Since different research has also demonstrated different optimal β values for different types of studies, it is also crucial to ascertain the optimum β values specifically suited for NCI, particularly for spatial resolution tests and clinical settings.

This study aims to address the knowledge gap regarding the enhancement of spatial resolution with increasing radial distances across the PET/CT FOV using alternative PSF models and BPL in OSEM algorithms while determining optimal β values for routine clinical use in NCI. Hence, it is essential to comprehend how spatial resolution is influenced by the radial distance within the PET/CT FOV and explore the role of different reconstruction techniques with alternative modelling methods to refine the imaging protocols and thus guarantee accurate diagnosis in clinical settings.

1.3 Study Objective

1.3.1 General Objectives

The aim of this study is to evaluate the impact of integrating PSF modelling and different BPL penalty functions to the radial spatial resolution within PET/CT field of view.

1.3.2 Specific Objective

1. To assess the impact of radial distances to the spatial resolution within PET/CT field of view.
2. To evaluate the ability of the PSF modelling and BPL penalty functions (β values) in retaining the spatial resolution at different radial distance within PET/CT field of view.
3. To optimize the BPL penalty functions (β values) in OSEM algorithms to improve the spatial resolution at different radial distances within PET/CT field of view.

1.4 Study Hypothesis

1.4.1 Null Hypothesis

1. There is no significant effect of radial distances to the spatial resolution within PET/CT field of view.
2. There is no significant effect of the PSF modelling and BPL penalty functions (β values) to retain the spatial resolution at difference radial distance within PET/CT field of view.
3. There is no significant effect of the BPL penalty functions (β values) in OSEM algorithms to improve the spatial resolution at different radial distance within PET/CT field of view.

1.4.2 Alternative Hypothesis

1. There is a significant effect of radial distances to the spatial resolution within PET/CT field of view.
2. There is a significant effect of the PSF modelling and BPL penalty functions (β values) to retain the spatial resolution at difference radial distance within PET/CT field of view.
3. There is a significant effect of the BPL penalty functions (β values) in OSEM algorithms to improve the spatial resolution at different radial distance within PET/CT field of view.

1.5 Significant of Study

The significance of the study includes the determination of spatial resolution from the center towards the periphery of the PET/CT FOV and determining the optimizing reconstruction parameters that can retain spatial resolution, especially at the edge of PET/CT FOV. Understanding the impact of TOF, PSF models and BPL penalty functions will contribute to the ongoing technological advancements in molecular imaging. In accordance with that, the findings of this study will contribute to the improvement of image analysis accuracy and the optimization of image acquisition techniques, particularly when analyzing structures at the periphery of the PET/CT FOV. In previous studies, different optimal β values have been recommended by different researchers and they are based on the different types of study protocols. Hence, this study will determine the optimal β value suitable for routine clinical application in NCI. This determination can significantly improve clinical decision-making accuracy, aiding in more precise diagnosis and treatment planning, subsequently improving patient outcomes and potentially reducing the necessity for

extra imaging. This might maximise resource utilisation and advance cost-effectiveness in healthcare. By pinpointing the optimal reconstruction techniques, this research advances the boundaries of achievable image quality and diagnostic capabilities of NCI.

1.6 Conceptual Framework

The independent variables of this study were different radial distances within PET/CT FOV and different reconstruction techniques like TOF, PSF modelling, and BPL penalty functions were applied in OSEM algorithms to calculate the dependent variables which were tangential and radial FWHM. Both tangential and radial FWHM are also known as transverse spatial resolution which the FWHM calculated were based on conventional point source method. Figure 1.1 illustrates the conceptual framework of this study.

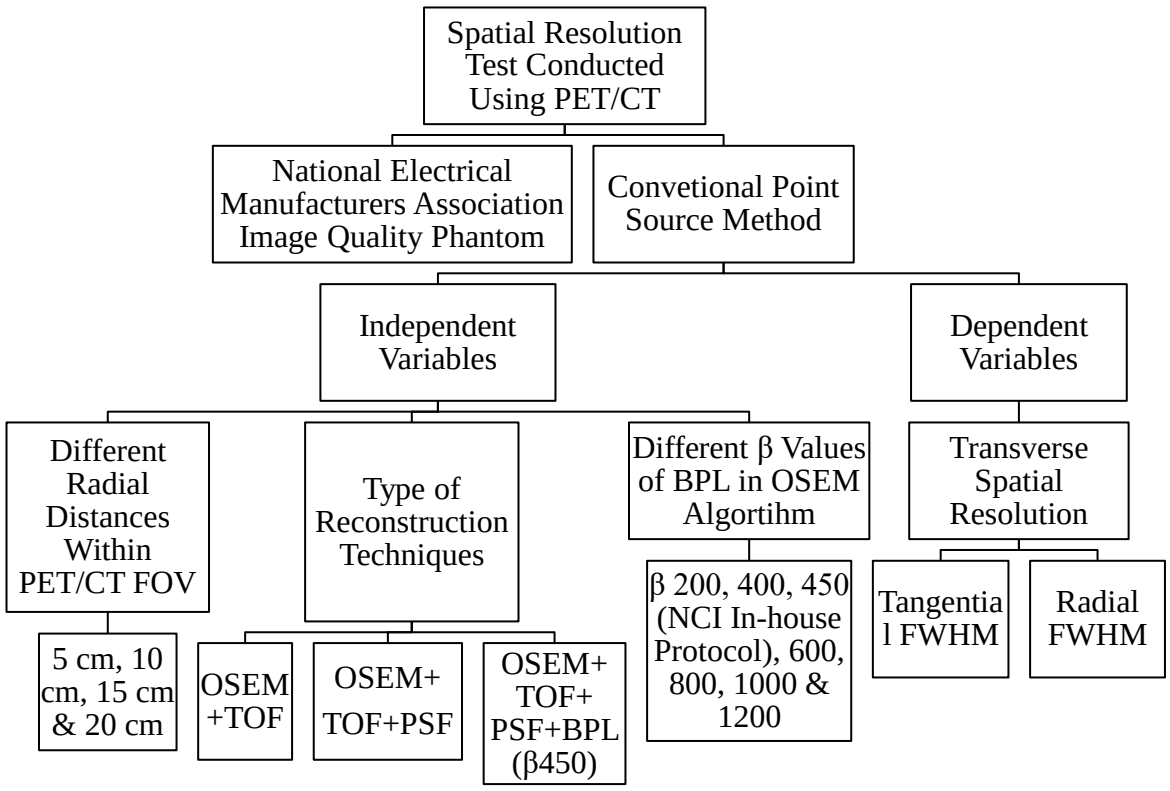

Figure 1.1: Conceptual framework

CHAPTER 2

LITERATURE REVIEW

2.1 Operational Principle of PET/CT

PET/CT is now becoming widely used in Nuclear Medicine due to its ability to detect two annihilation coincidence photons when a positron interacts with an ordinary electron. Before PET/CT imaging, radiotracer is administered to the patient, and it will accumulate more in areas with high levels of metabolism and glycolysis. When the radiotracer decays, it releases positrons which the positrons will then interact with electrons in the body, converting masses of both particles into energy. The energy resulting from the annihilation process is the emission of two photons, each with 511 keV energy. The photons will then leave the annihilation point in opposite directions at approximately 180˚ each other (Cherry et al., 2012).

PET scanners are commonly made up of a full ring of modular block detectors that record the simultaneous detection of two photons or known as coincidence pair which provide information about the distribution of the activity in the body. If the two photons interact with the detectors, the annihilation position is somewhere along the line connecting the two interactions which is known as the line of response (LOR). The PET images are reconstructed by processing the PET data using OSEM algorithms. The PET scanner is also combined with CT scanner to provide anatomical information which is fused with PET image to provide a detailed understanding of internal body anatomical information and metabolic activity (Shukla & Kumar, 2006).

2.2 Spatial Resolution in PET/CT Field of View (FOV)

FWHM of a point source or line source which is expressed in millimetres (mm), is typically used to prepare for spatial resolution tests. According to the study

conducted by Gong et al. (2016), spatial resolution can be measured by reconstructing the point source scans using FBP or OSEM algorithm and then obtained FWHM from line profiles and calculating. FWHM is obtained by measuring the width of the peak on the line profile and it functions to determine the energy resolution of the detector (*Energy Resolution,* n.d.). Spatial resolution is theoretically quantified as FWHM measurement on the line profile of counts versus distance (*NM Image Quality - Radiology Cafe*, 2021). Smaller FWHM indicates better resolution of the PET system. The spatial resolution of point sources is evaluated by examining the FWHM of the line profile. On the other hand, the spatial resolution for line sources is assessed by the FWHM of the Line Spread Function (LSF), which represents the count distribution in a line perpendicular to the source image (*Spatial Resolution,* n.d.).

In theory, the resolution is better through the center of PET FOV than the periphery of FOV. This has been proved by a few researchers such as Smith et al. (2023) and Yamagishi et al. (2023) had conducted the spatial resolution test by utilizing F-18 point sources with activity > 200 MBq/ml and > 500 MBq/ml respectively. Three-point sources are positioned radial offsets of 1 cm, 10 cm, and 20 cm from the center of the PET/CT FOV. The primary difference between both studies is that Smith et al. (2023) acquired PET images until they achieved over 500,000 counts, while the point sources were scanned for 1 minute for study by Yamagishi et al. (2023). Both studies utilized the OSEM algorithm to reconstruct the image but Yamagishi et al.'s study performed FBP reconstruction as well to evaluate the spatial resolution of the point sources from the center towards the edges of the PET/CT FOV.

From the result of tangential FWHM obtained at 1 cm, 10 cm and 20 cm radial offset, Smith et al.'s study demonstrated 3.76 mm, 3.85 mm, and 4.19 mm respectively while Yamagishi et al.'s study revealed 3.73 mm, 3.90 mm and 4.26 mm respectively.

Based on the result clearly shows that an increase in radial distance results in increases FWHM values which indicates that degrade in spatial resolution. According to the image reconstructed using FBP, the tangential FWHM calculated at 1 cm, 10 cm and 20 cm radial offset are 4.22 mm, 4.55 mm, and 5.03 mm respectively. It also clearly shows that images reconstructed using the OSEM algorithm show better in recovering the spatial resolution loss compared to images reconstructed using FBP.

2.3 Fundamental Limitations of PET/CT in Spatial Resolution

There are some fundamental factors affecting spatial resolution such as matrix size, voxel size and PET detector design. A decrease in matrix size will increase spatial resolution. This is because increasing matrix size will result in smaller pixel size and smaller pixel size will thus increase the spatial resolution as each pixel can capture finer details. Additionally, the reconstructed image's spatial resolution will be impacted by the dimensions of its 3D pixels or known as voxels. The dimensions of a voxel are ascertained by multiplying its pixel size in x and y on the 2D detector by its slice thickness in z dimensions. This results in the volume of the voxel. The spatial resolution increases with decreasing voxel size but there's a chance that this will make images noisier.

Moreover, full ring of modular block detector design is now widely used as it can result in high sensitivity and reduce motion artefacts. This full ring block detectors of PET scanners are made up of 24 to 32 rings of detectors with hundreds of crystal elements per ring which enable millions of data to be processed. Block detector design also allows smaller detector elements of PET to be used. This allows better localization of gamma ray interaction position and eventually improves the spatial resolution (Cherry et al., 2012).

Nevertheless, spatial resolution within the PET FOV is non-uniform as it degrades from the center towards the edge of the FOV. Spatial resolution in PET is generally limited by several natural physical factors and detectors related effects. Natural physical factors include positron range and annihilation photons non-collinearity. Meanwhile, detectors related effects include width of scintillation detectors, inter-crystal scattering, inter-crystal penetration, decoding, and sampling errors (Moses, 2011). Although some efforts have been made by research to address the limitation of spatial resolution in PET/CT, several limitations can be reduced but cannot be solved.

2.3.1 Natural Physical Limitation

2.3.1.1 Positron Range

The positron range is defined as the average distances travelled by positrons in a medium before they can reach thermal energies to be annihilated in the PET/CT scanner (Moses, 2011). The occurrence of the positron range is due to the type of isotope and type of medium that positron travel. To increase the spatial resolution, the smallest mean positron range in water is preferable. F-18 gives the smallest positron range in water among several types of isotopes as shown in Table 2.1, in which the mean positron water range in water is 1.0 mm.

Besides, spatial resolution can be improved in a higher tissue density which subsequently results in decreasing the positron range. This is because in a higher density medium, the positron is hard to be transmitted through the medium, hence positron range is lower in a higher density medium. Figure 2.1 shows lower density medium (lung) results in a higher positron range in which the point source appears broader in size. A small discrepancy between the actual and measured positions of positron emission may arise from the positron range. The amount of visual blurring

that results from this will vary depending on the activity of the parent radioisotope. To put it briefly, the lower the positron range, the smaller the deviation between the parent and detected position of the positron emission and hence result in better image spatial resolution (Aklan et al., 2015; Moses, 2011).

Table 2.1 Characteristic of Commonly Used Positron Emitting Isotopes (Kevrešan, n.d.).

Isotopes	Half-Life (mins)	Positron Range in Water (FWHM in mm)
Carbon-11	20.3	1.1
Nitrogen-13	9.97	1.4
Oxygen-15	2.03	1.5
Fluorine-18	110	1.0
Gallium-68	67.8	1.7
Rubidium-82	1.26	1.7

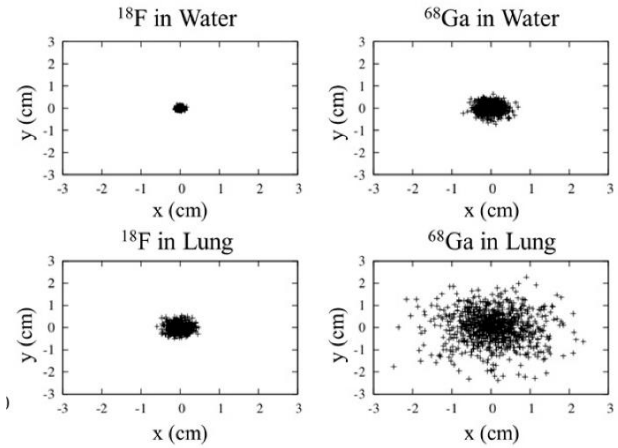

Figure 2.1: Different type of medium in affecting positron range (Herraiz et al., 2020).

2.3.1.2 Photon non-collinearity

Photon non-collinearity is defined as a small angle difference between the two photons from 180˚ during the annihilation process (Moses, 2011). The momentum of

the center mass is zero during the annihilation when the kinetic energy of the electron and positron is likewise zero. Due to momentum conservation, when a photon is released, its momentum is preserved, causing both photons to be released at a 180˚ angle and in the opposite direction. The residual momentum of the positron at the end of its trajectory in a medium caused a little departure of 0.25˚ from the theoretical expectation that two photons would be released precisely 180˚ apart in opposing directions as shown in Figure 2.2. This incident will eventually affect the spatial resolution due to the error that occurred in the LOR definition (Cherry et al., 2012). Because the PET detector is divided into smaller detector parts, a tiny angle change caused by photon non-collinearity may result in an error in the LOR.

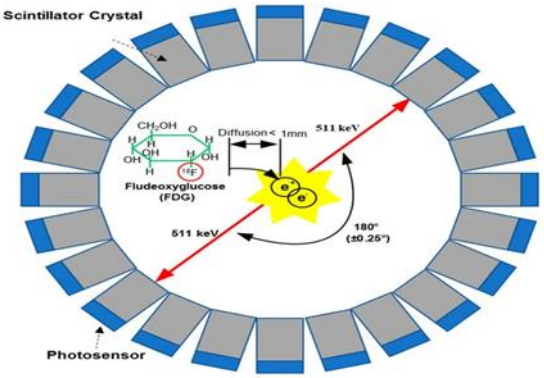

Figure 2.2: Basic principle of PET with occurrence of photon non-collinearity (Jiang et al., 2019).

2.3.2 Detector Related Effects

2.3.2.1 Width of scintillation crystals

The location of annihilation events inside the scanner field of view determines the intrinsic resolution. The spatial resolution improves with decreasing PET detector size but will reduce the sensitivity of the system. The optimal crystal size and thickness also depend on the specific application and imaging requirement. Scintillation crystals with strong light output and emission spectra that match the photodetectors' sensitivity

wavelength are necessary for high-spatial resolution PET scanners. Detectors composed of lutetium oxyorthosilicate (LSO) or lutetium yttrium oxyorthosilicate (LYSO) are typically utilized to obtain high spatial resolution. Zhang Xi and the team have developed a PET detector composed of LYSO with a 0.5 mm crystal pitch intended for high-resolution preclinical imaging (X. Zhang et al., 2021). The distance between the center of neighbouring crystals in the detector array is called crystal pitch. The lower the crystal pitch, the closer together the crystals are grouped. The crystals are arranged closer together the smaller the crystal pitch. Based on the PET detector's performance, the most consistent flood map created by detected signals is obtained when the light guide's thickness is set at 2.35 mm (X. Zhang et al., 2021).

2.3.2.2 Inter-crystal scattering and penetration

Inter-crystal scattering and penetration are the processes by which a photon travels through a crystal and is detected in a different detector rather than interacting with it at one particular location as illustrated in Figure 2.3. Photons that entered the crystal at angles other than perpendicular to it were said to cause inter-crystal penetration or ICP. A phenomenon called parallax effect occurs when ICP effects become more noticeable near the edge of PET/CT FOV. However, inter-crystal scattering (ICS) might occur even though photons entered the crystal perpendicularly. This is because photons undergo Compton scattering, which causes photons to scatter from one crystal to the next, depositing some of their energy in one or more of the crystals (Lee & Lee, 2021). As a result, the quality of the image deteriorates, and the spatial resolution is decreased because the photon was initially absorbed in an incorrect crystal (Zeraatkar. N et al., 2011).

For 511 keV gamma photons, there is a high likelihood of ICS events in all contemporary scintillation crystals (C. Zhang et al., 2019). Because certain photons

are detected in crystals that do not match the point of annihilation from whence the photon emanated, both ICS and ICP lead to a deterioration of spatial resolution. Inaccurate LORs are most likely described as one or two photons that are misplaced because of ICS and ICP. Studies found that researchers have introduced and employed convolution neural networks and Monte Carlo simulations to assess and recover the impact of ICS on PET detectors (Lee & Lee, 2021; Zeraatkar. N et al., 2011).

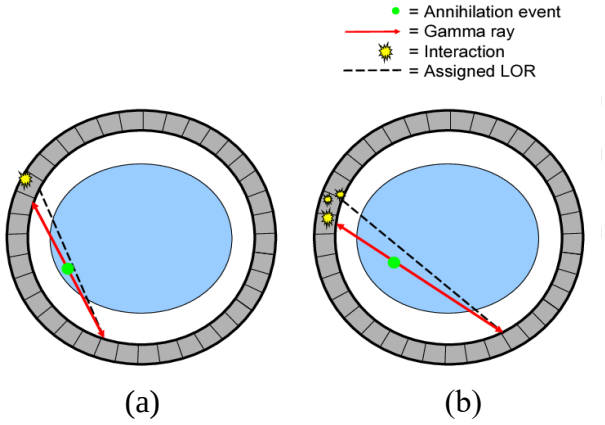

Figure 2.3: (a) Inter-crystal Scattering; (b) Inter-crystal Penetration (Iriarte et al., 2015)

2.3.2.3 Decoding

In PET/CT, decoding is the process of creating an image by converting the electrical impulses produced by the detectors into digital signals. The location of the scintillation event in the detector and the energy deposited by the gamma ray are the two steps in the decoding process. To decrease the number of electronic channels, most PET detectors employ optical multiplexing, which involves placing more scintillation crystals than photodetector elements. Nevertheless, the drawback of decoding is that it will be expensive because of the rise in photodetectors, electronic channels, and building complexity (Moses, 2011).

2.3.2.4 Sampling Errors

Sampling error in PET/CT normally is caused by the limited number of detected coincident events in the PET/CT scanner (Moses, 2011). In PET/CT, the two coincidence photons emitted from the positron-electron annihilation when interacting with detectors. The sampling error arises because the LORs are spaced uniformly which is separated by crystal width (Surti et al., 2009). Commonly, sampling errors happen in the vicinity of the camera's center as illustrated in Figure 2.4. This occurs because certain pixels in the FOV have a high LOR transit rate while others have a low LOR transit rate. Due to non-uniformity sampling, this may result in a reduction in spatial resolution. Surti and the team have developed techniques to improve the sampling in pixelated detectors and produce findings that are more in line with theoretical estimations (Surti et al., 2009).

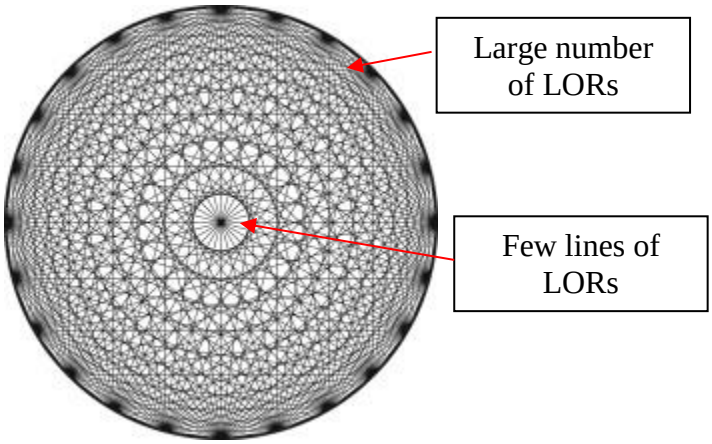

Figure 2.4: LORs in PET camera (Moses, 2011)

2.4 Spatial Resolution Recovery by Reconstruction Algorithms

An effective strategy for addressing the limitations of PET/CT involves the implementation of reconstruction algorithms. Advanced reconstruction algorithms have been used since the 1990s to increase PET's spatial resolution (Tong et al., 2010). In the past, FBP was typically used for PET image reconstructions due to its quick computing speed. One of the drawbacks of employing FBP is that reconstruction

accuracy is constrained by the technology's capacity to account for attenuation and scattering, as well as by inherent physical limitations of PET, such as photon non-collinearity and positron range (Kumar Jha et al., 2014). Due to this constraint, the iterative reconstruction technique was developed and is now a common feature of most commercial PET/CT scanners. There are a few types of reconstruction algorithms such as OSEM with the help of TOF, alternative PSF modelling and different beta penalizing functions. Different vendors use different terminology for image reconstruction methods which can be shown in Table 2.2.

Table 2.2: Different terminology for different image reconstruction methods coined by different vendors.

	GE Discovery	Siemens Biograph
OSEM	Vue Point HD (VPHD) ➢ OSEM (non-TOF)	HD ➢ OSEM2D or OSEM3D
Time of Flight (TOF)	Vue Point FX (VPFX) ➢ OSEM + TOF	UltraHD
Point Spread Function (PSF)	SharpIR ➢ Usable for both VPHD and VPFX	TrueX ➢ Usable for both HD and UltraHD

2.4.1 Ordered Subset Expectation Maximization (OSEM) Algorithm

OSEM reconstruction algorithm is introduced and is mostly utilized in nuclear medicine since the drawbacks of MLEM outweigh its benefits (Hudson & Larkin, 1994). MLEM is time consuming due to slow convergence because each iteration requires one forward projection of the estimate and one back projection of the entire data set. The FBP on back projection reconstructs all the data set with around half of the time needed for 1 MLEM iteration (Gaitanis et al., 2010). MLEM reconstruction will also degrade the image resolution due to more iterations that result in the noisier image (Iterative Reconstruction, n.d.). Meanwhile, every update for OSEM only uses

a subset of projection angles since projection data is separated into ordered subsets, each of which has an equal number of projections, in contrast to MLEM which uses back projection and forward projection for every projection angle.

Subsequently, each estimated subset is updated to a new estimated subset by comparison with its measured subset. However, the OSEM algorithm does not provide the full convergence of projection data to the maximum probability because the noise in the image tends to grow with each iteration thus impacting the image quality (Ross, 2014; te Riet et al., 2019). To address this issue, the algorithm will stop after a predetermined number of iterations, normally two to four iterations. This can keep the noise from being overly noticeable, but quantitative accuracy will decrease and cause an under-converged image or small object distortion (Ross, 2014).

2.4.2 Time of Flight (TOF)

OSEM can be used with TOF for better localization of annihilation events and thus improving the SNR in reconstructed images. TOF measures the time takes for a pair of gamma rays to reach the detectors after the annihilation process that results in the emission of a positron. TOF can accurately determine the origin of gamma rays and thus result in improved spatial localization and image quality. It can improve image quality by reducing the background noise and thus improve quantitative accuracy (*VUE Point FX,* n.d.). Based on the study conducted by Lodge et al. (2018), F-18 point source was placed at 10 cm radial offset from the center of PET/CT FOV and the image was then reconstructed with Fourier rebinning plus FBP (FORE+FBP) and OSEM+TOF. The result shows that OSEM+TOF provided better spatial resolution than FORE+FBP. The study also shows that FWHM degraded with increasing radial distance and depended on the reconstruction algorithms (Lodge et al., 2018).

In a conventional PET system, annihilation is assumed to occur at the midpoint of the two detectors or equal probability for the recorded event along the LOR. The time of arrival of the two photons would be similar ($t_1 = t_2$). Nevertheless, data loss and poor photon detectability might occur if the annihilation or point of interaction occurs away from the center of the two detectors rather than at their midpoint since two photons will be detected at a different moment ($t_1 \neq t_2$) as depicted in Figure 2.5. Photons that are in closer proximity to detectors will arrive more quickly than those that are farther away. If the time difference between the two photons to reach the detectors is bigger than the coincidence time window, the system will reject this event.

To resolve this issue, TOF is introduced which the precise time that each of the coincidence photons is detected is noted by calculating the difference in arrival time and performing correction. TOF considers the variation in arrival time between two photons (Cherry et al., 2012). The position of annihilation is then localized by calculating the displacement location based on the variations in arrival timings. The difference in arrival times aids in pinpointing the annihilation event's location along the LOR since the closer photon will reach the detector sooner. The emission distance along the LOR, d is determined by Equation 1.

$$t_2 - t_1 = \frac{2\,\Delta d}{c}$$

$$d = \frac{c\,(t_2 - t_1)}{2} \qquad (1)$$

Where c is the speed of light, t_1 is the arrival time on the first detector and t_2 is the arrival time on the second detector. Thus, TOF allows for the localization of the annihilation process on the LOR, in contrast to conventional PET. This aids in strengthening the hotspot's structural definition and lesion detectability.

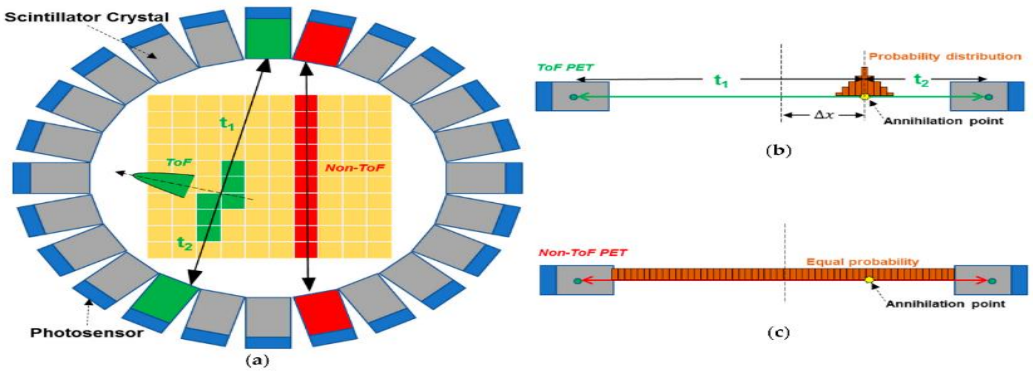

Figure 2.5: Concept of TOF PET and Non-TOF PET (Jiang et al., 2019).

2.4.3 Point Spread Function (PSF) Modelling

Point Spread Function (PSF) modelling is a method used to improve spatial resolution and quantitative accuracy in PET images (Murata et al., 2016). It is based on theoretical derivation, analytical approximation, computer simulation or experimental measurements then incorporated into an iterative image reconstruction process (Cui & Gonzalez, 2018). Different vendors coin PSF correction software with different terminology. For instance, GE names PSF modelling as SharpIR which utilizes Monte Carlo simulations. PSF modelling has been demonstrated to improve spatial resolution and quantitative accuracy in PET images compared to OSEM and OSEM+TOF as shown in Figure 2.6 which illustrates PSMA uptake in the prostate and four metastases. PSF modelling can assist in reducing the blurring effect caused by the physical characteristics of the PET system and result in sharper and more accurate images.

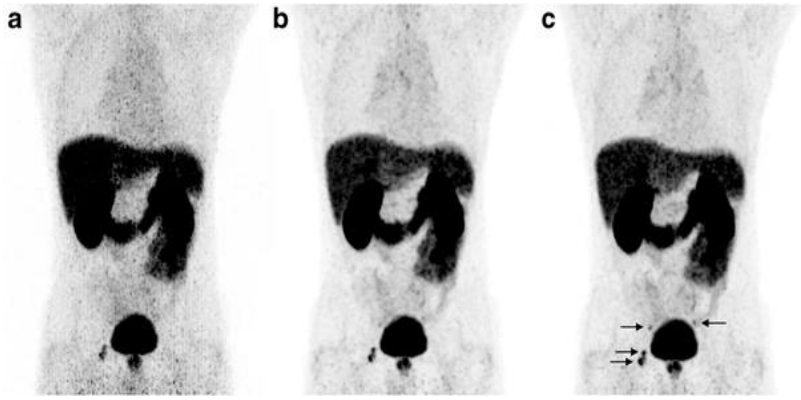

Figure 2.6: ^{68}Ga-prostate-specific membrane antigen (PSMA) PET images that shows the uptake of PSMA in prostate and four metastases. PET data is reconstructed with (a) OSEM, (b) OSEM+PSF and (c) OSEM+TOF+PSF (van der Vos et al., 2017).

The introduction of PSF modelling is due to the fundamental limits of PET/CT systems which eventually lead to the non-uniformity in resolution within the FOV and degrade the spatial resolution at the edges of FOV (You et al., 2019). The PSF addresses issues like the mispositioning of photons known as the parallax effect due to ICP that happens when gamma rays enter the scintillation detectors in both non-oblique and oblique angles. It also corrects for factors like ICP and ICS, positron range and photon non-collinearity (Aklan et al., 2015). PSF modelling is essential as all these fundamental limitations of PET/CT will impact the spatial resolution and quantitative accuracy in PET/CT images when it comes to an increase in the radial distance from the isocenter.

Several studies have demonstrated that incorporating PSF information into several reconstruction algorithms such as OSEM and TOF can improve image quality in terms of spatial resolution. The National Electrical Manufacturers Association (NEMA) image quality phantom filled with a 4:1 signal-to-background ratio was used in an experimental study by Vennart et al. (2017) to measure whether PSF modelling addition to the OSEM and TOF algorithms yielded any improvements. The sample of

15 whole-body ^{18}F-FDG scans were reconstructed with OSEM, OSEM+TOF and OSEM+TOF+PSF which the outcomes demonstrated that PSF reconstruction greatly enhanced the image quality for phantom and clinical investigations.

Apart from that, some studies have been carried out to evaluate the FWHM of point sources with the effects of PSF correction at various locations along the PET/CT FOV. Murata et al. (2016) performed the spatial resolution test by using a Na-22 point source with activity > 1 MBq/ml. The point source was positioned in three directions (x, y and xy axes) at intervals of 1 cm from center towards the peripheral FOV with data acquired for 2 minutes per point. The PET data were then reconstructed using FBP, OSEM, OSEM+TOF+PSF, and OSEM+PSF to determine the optimal reconstruction techniques for yielding the best spatial resolution. The findings demonstrated that the FWHM of point sources reconstructed with FBP and OSEM increased towards the edge of PET/CT FOV. In contrast, PSF modelling effectively recovered the FWHM at every point in the FOV. Specifically, the FWHM of the point source reconstructed with OSEM+PSF and OSEM+TOF+PSF was 30% to 50% lower than the point source reconstructed using OSEM at the center of FOV.

Another study by Chicheportiche et al. (2020) also proved that incorporating PSF modelling into the OSEM algorithm improves spatial resolution within PET/CT FOV. Unlike Murata et al.'s study, Chicheportiche et al. placed three F-18 point sources with activity of 1.5 MBq/ml at radial distances of 1cm, 10 cm and 20 cm. The PET data was then acquired for 1 min and the image was then reconstructed with FBP, OSEM and OSEM+PSF. The result showed that OSEM+PSF resulted in better spatial resolution within the PET/CT FOV as the tangential FWHM of the point source at 1 cm, 10 cm and 20 cm radial offset were 4.52 mm, 4.90 mm and 4.90 for FBP, 3.89 mm, 3.98 mm and 4.06 mm for OSEM algorithm as well as 2.82 mm, 2.72 mm and 2.75

mm for OSEM+PSF. Both F-18 and Na-22 can be utilized to prepare point sources with activity low enough that at least the percentage of dead time losses is less than 5 %, or the random coincidence rate is less than five percent of the overall event rate, in accordance with NEMA NU-2 2018 criteria. In short, integrating PSF modelling in OSEM algorithms has shown improvement in spatial resolution within the PET/CT FOV.

2.4.4 Bayesian Penalized Likelihood (BPL)

Since OSEM cannot provide the full convergence of projection data, came to the introduction of smooth penalty function Bayesian Penalized Likelihood (BPL) which can perform a regularized iterative reconstruction. It is a new reconstruction algorithm known as BSREM. BSREM is based on OSEM algorithms but includes BPL algorithms which add penalty or regularization terms to improve image quality and allow each voxel to achieve full convergence (te Riet et al., 2019). GE Healthcare unveiled BPL with software named Q.Clear. PSF modelling is integrated into BSREM reconstruction. Q.Clear also known as BPL which is a function to reduce the noise from the optimized image and allow each voxel to achieve full convergence (Assaf et al., n.d.). In comparison to OSEM, it offers improved SNR and SUV recovery along with more precise quantitation levels as shown in Figure 2.4 (Ross, 2014).

BPL is defined by: $\phi(\chi) = \sum_i y_i \log([P_x]_i + r_i) - ([P_x]_i) - \beta R\,(x)$ (2)

where x is the activity image, y_i represents the emission sinogram data, P includes the forward projection operator involving attenuation, normalization and PSF resolution modelling, r_i denotes the estimated background contributions from scatter and randoms, $R(x)$ signifies penalty function, and β serves as the regularization or penalty parameter governing the overall strength of regularization (Yamaguchi et al., 2018).

The BPL algorithm is utilized to evaluate the small lesion detectability, SUV recovery and noise suppression in most of the study. Research has shown that the OSEM+TOF+PSF+BPL algorithm results in better recovery in small lesions based on images of 100 million counts acquisition of NEMA image quality and ^{18}F–FDG PET images of patient with ovarian cancer with peritoneal carcinomatosis. Both PET data are reconstructed with OSEM, OSEM+TOF+PSF and OSEM+TOF+PSF+BPL (β400) which is illustrated in Figure 2.7. Furthermore, the research done by Howard and the team proved that the BPL algorithm enables the lung nodules SUV to be clearly visualized and the SUV maximum values of tiny nodules measuring 10 mm or smaller might be increased. 100% convergence is made possible with a greater SNR (Howard et al., 2017). In addition, Howard also suggests that the BPL algorithm makes lesions more noticeable than low noise penalization non-TOF OSEM.

From the research done by Vallot et al. (2017) to evaluate the effect of BPL reconstruction algorithms on PET FDG metrics, the BPL algorithm can significantly improve the image quality and lesion contrast, particularly for patients with high body mass index (BMI). In essence, the penalty term in both Q.Clear and PSF modelling allows for the control of noise, leading to less smoothing in higher activity zones and less noise in lower activity parts. In short, both can smoothen the cold backgrounds and improve the hot lesions SNR.